Proceedings of the 2nd Winter Workshop S&SRES'96, Polanica Zdrój 1996

MULTIPHONON ABSORPTION AND PHOTON AVALANCHE CRITERION IN ERBIUM DOPED MATERIALS

F. AUZEL

France-telecom, CNET PAB/BAG-Laboratoire de Bagneux, Groupe Optique des Terres-rares, B.P.107, 92225, Bagneux, France

The photon avalanche effect has been recently observed at room temperature in erbium doped fluoride glasses and crystals, in a particularly clear way, displaying simultaneously all the typical features of this effect: (i) existence of a threshold for transmission at the excitation wavelength, (ii) up-conversion excitation threshold, (iii) long delay for threshold establishment. Analysing the first step of the avalanche effect as an anti-Stokes multiphonon absorption, it can be shown why this effect is so clearly observed at room temperature in our erbium studies. Our results are compared with other cases of avalanche, with cases which have been called "looping effects" and "quasi-avalanche" ones.

PACS numbers: 42.50.Hz, 42.62.Fi, 42.70.Ilj, 78.50.Ec

1. Introduction

The photon avalanche effect has been recently observed at room temperature in erbium doped fluoride glasses [1–4] and crystals [5], in a particularly clear way, displaying simultaneously all the typical features of this effect: (i) existence of a threshold for transmission at the excitation wavelength, (ii) an up-conversion excitation threshold, (iii) a long delay for threshold establishment. Such peculiar behaviour had been first observed below 40 K in Pr^{3+}-doped $LaCl_3$ and $LaBr_3$ crystals [6, 7]. Soon afterwards, the avalanche pumped laser effect had been obtained in Pr^{3+}:$LaCl_3$ [8]. Quite recently it has been also observed in Er^{3+}:$YALO_3$ [9, 10] but all of them also below 40 K. Some of the features of the avalanche effect have been observed at room temperature in a Pr^{3+}-doped silica glass fiber [11].

In many cases the initial first step for avalanche was not considered, the theoretical analysis starting with an already populated metastable state. Such a "by-pass", usually considered for simplification, hides some of the interesting features of the avalanche process, in particular the condition of existence of a meaningful experimental threshold.

Analysing the first step of the avalanche effect as an anti-Stokes multiphonon absorption and using the simplified approach of Goldner and Pellé [12], it can

be shown why this effect is so clearly observed at room temperature in our erbium studies [1–5]. We shall compare our results numerically with other cases of avalanche [10] or with cases which have been called "looping effects" [14] or "quasi-avalanche" ones [15].

2. The basic photon avalanche process

While looking for 2-step absorption in Pr^{3+}-doped $LaCl_3$ and $LaBr_3$ at low temperature (< 40 K) as a mean to detect an IR photon by its energy summation with a more energetic photon so performing excited state absorption (ESA), it was found that the higher energy photon alone could, in the same time, give rise to up-conversion and reduce the transmission of the sample above a given intensity threshold [6], see Fig. 1. The effect was attributed to an increase in population on an excited state resulting from a cross-relaxation process. The starting process was initially not completely determined. In the Pr^{3+} case, the $^3H_5 \rightarrow {}^3P_1$ absorption is initially very weak at low temperature because $^3H_5$ is about 2000 cm^{-1} above the ground state (see Fig. 2); however above about 1 mW of excitation this transition is increased; the cross-relaxation $(^3H_6,\ ^3H_4) \rightarrow (^3H_5,\ ^3H_5)$ increasing the $^3H_5$ population which in turn reduces the transparency of the sample at the $(^3P_1 - {}^3H_5)$ energy. Since the more the $(^3P_1 - {}^3H_5)$ energy is absorbed the more the $^3H_5$ population is increased, the process was termed "photon avalanche" [6]. It is a clear way to increase ESA in a sample.

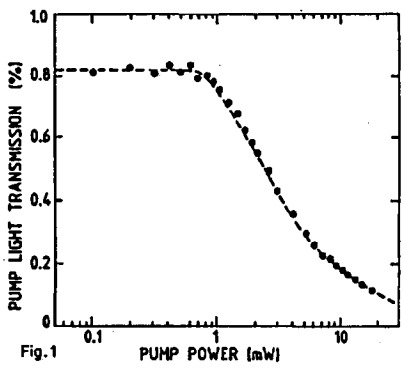

Fig. 1

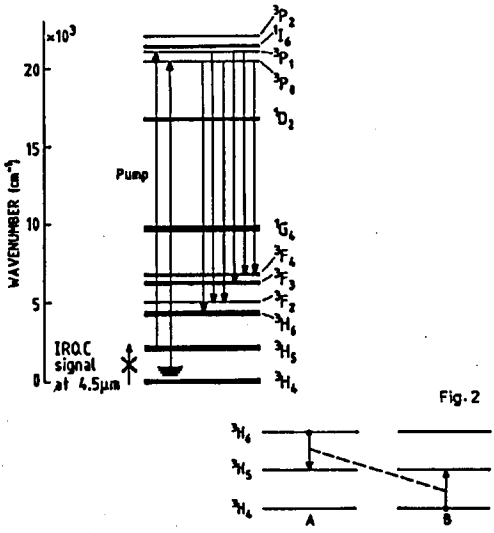

Fig. 2

Fig. 1. Decrease of transmission in a Pr^{3+}:$LaCl_3$ sample under $^3H_5 - {}^3P_1$ pumping, after [6].

Fig. 2. Pr^{3+} energy levels involved in the avalanche process, after [6].

Afterwards, similar effects have been observed in Sm^{3+}, Nd^{3+}, Ni^{2+}, Tm^{3+} doped halide crystals [16–19]. Recently we obtained the photon avalanche effect at

room temperature for the Er^{3+} ion in a ZBLAN (ZrF_4, BaF_2, LaF_3, AlF_3, NaF) glass both in bulk and in fiber form [1–4] and in a $LiYF_4$ crystal [5].

As already said, there are three distinct aspects for the photon avalanche process non-linear behaviour: (i) transmission, (ii) emission and (iii) rise time on the pump power intensity generally with the existence of a critical pump threshold.

Particularly long rise times, from seconds to minutes [5, 20] have been observed.

3. Existence of a threshold

At this point it is worth discussing the notion of threshold for avalanche. Due to the complexity of the phenomena, it has been usually modelled by a simplified three-level system [21, 22, 12]

3.1. The avalanche process as a positive feed-back system

Using the 3-level simplified model of [21] or [22] and adding to the initial ground state absorption ($\sigma_1\Phi = R_1$) an auxiliary direct feeding into the metastable state ($\sigma_0\Phi_{IR}$) we may write the following set of equations (see Fig. 3 for explanation of symbols which except for the trigger $\sigma_0\Phi_{IR}$ are the same as in Ref. [21]).

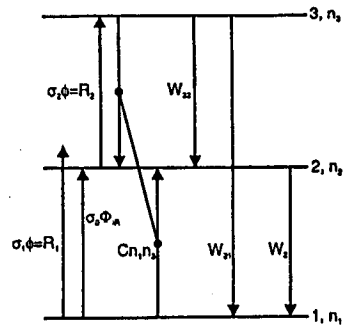

Fig. 3. The avalanche simplified 3-level scheme, C is the cross-relaxation coefficient, W_{ij} are the spontaneous emission terms.

Being interested in the steady state initial step of avalanche we assume

(i) $\dfrac{dn_1}{dt} = \dfrac{dn_2}{dt} = \dfrac{dn_3}{dt} = 0,$

(ii) $n_1 = 1 - n_2 - n_3 \approx 1.$

Then the rate equations are simplified to

$$0 = -R_1 - \sigma_0\Phi_{IR} + bW_3n_3 + W_2n_2 - Cn_3, \tag{1}$$

$$0 = (1-b)W_3n_3 - W_2n_2 + 2Cn_3 + R_1 + \sigma_0\Phi_{IR} - R_2n_2, \tag{2}$$

$$0 = R_2n_2 - W_3n_3 - Cn_3 \tag{3}$$

with C the cross-relaxation parameter and b — the branching ratio. The following relationships exist between the transition probabilities:

$$(1-b)W_3 = W_{32}; \qquad bW_3 = W_{31}; \qquad W_3 = W_{32} + W_{31}$$

and Eq. (3) can be written as

$$n_2 \frac{R_2}{W_3 + C} = n_3. \tag{3'}$$

Or considering amplitude and using the symbolic representation for feed-back systems (3') give the block A in Fig. 4a.

In the same way Eq. (1) is written as

$$n_2 = \frac{R_1 + \sigma_0 \Phi_{IR}}{W_2} + \frac{C - bW_3}{W_2} n_3, \tag{1'}$$

which can be symbolised in Fig. 4a by the block β and adder with the input source $(R_1 + \sigma_0 \Phi_{IR})/W_2$.

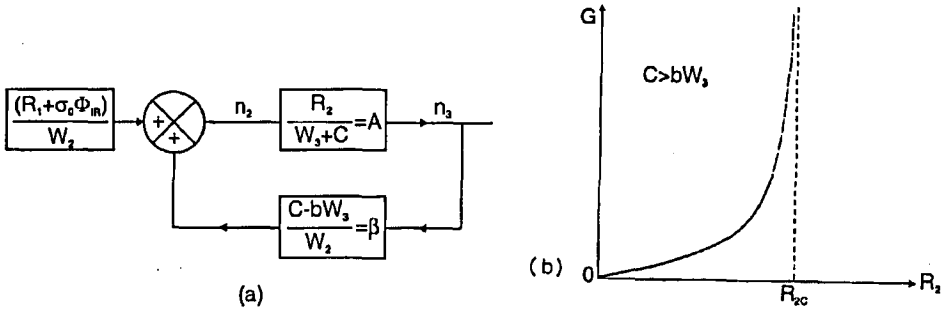

Fig. 4. (a) Positive feed-back model for avalanche. (b) Gain behaviour of the model versus R_2; positive feed-back condition is $b > CW_3$, the asymptote R_{2C} corresponds to the avalanche threshold.

Combining (1') and (3') gives the classical feed-back system scheme in Fig. 4a. Such system is known to be unstable for $A\beta = 1$. One can define a "gain" of the closed loop feed-back system, G, by the ratio between the green output to a pump related input signal (R_1) plus an eventual trigger (Φ_{IR})

$$G = \frac{n_3}{(R_1 + \sigma_0 \Phi_{IR})/W_2}. \tag{5}$$

It is well known that in term of A and β in Fig. 4a, one has

$$G = \frac{A}{1 - A\beta}. \tag{5'}$$

The stability condition is then written as

$$\frac{R_2}{W_3 + C} \frac{C - bW_3}{W_2} < 1, \tag{6}$$

its limit is just the threshold condition given by Joubert et al. [21] obtained here in a simplified way

$$R_{2C} = \frac{W_2(W_3 + C)}{C - bW_3} \tag{6'}$$

with $C > bW_3$ for a positive feed-back.

The behaviour of our feed-back system below the threshold can be described by the behaviour of $G(R_2)$, Fig. 4b.

The feed-back "black box" approach has been also considered while studying the dynamics of the above three-level system [23]. It is based on the fact that the general feed-back linear theory used to solve algebraically time variable differential equation systems by using the Laplace transform of the time dependent functions.

3.2. Conditions to observe a threshold

With neglect of the first non-resonant absorption step (R_1) and taking into account only the second resonant absorption step (R_2) the calculation of the population of the third level (n_3) versus R_2 (the pumping excitation) leads to a well-defined non-linearity in n_3; the asymptotic curve in Fig. 5.

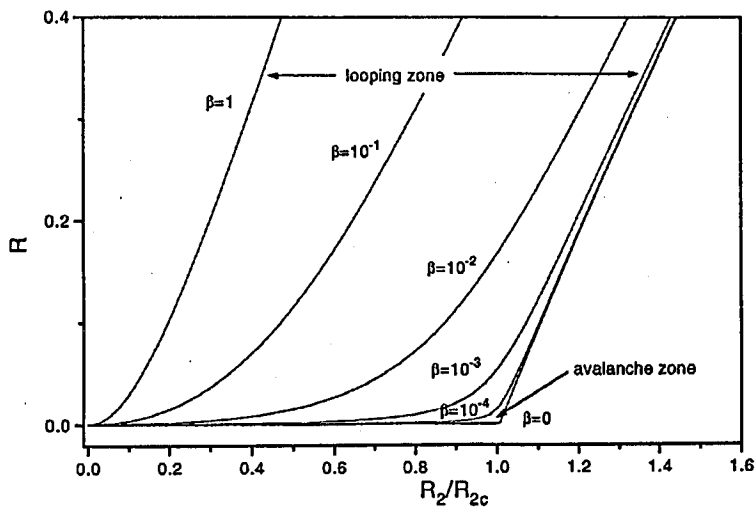

Fig. 5. The third level normalised population, $R = n_3(\beta, R_2)/n_3(\beta = 1, R_2 = R_{2C})$, versus pumping term ($R_2$) with β as a parameter, after [12].

When the first step (R_1) is explicitly taken into account [12], the "threshold" non-linearity is progressively smoothed out when the ratio $\beta = R_1/R_2$ is increased as shown in Fig. 5. This corresponds to a progressively more resonant first step. Practically a clear avalanche threshold can be expected only for β ratios $\leq 10^{-4}$ [12].

Some of the features of the avalanche effect have been observed at room temperature in Tm^{3+}:$YAlO_3$ [19] and in Pr^{3+} in silica glass fibres [11]. The lack of a clear threshold in this two systems can certainly be related to the above prediction.

The region in Fig. 5, where $10^{-4} < \beta < 1$, corresponds to cases for which the losses in the feed-back loop may exceed the loop gain for R_2 values below R_{2C}, so that after a number of "looping" of the excited population between level 3 and the metastable level 2, the system would not diverge and maintain n_3 independently of R_1. Such cases have been called "looping mechanism" [14] and we believe that some of the reported cases of quasi-zero threshold avalanche cases in the literature [11, 15] belong to large $10^{-3} < \beta \leq 1$ cases for which, as shown in Fig. 5, it is very difficult to distinguish between avalanche and sequential two-photon absorption (ESA). Sometimes they have been termed "quasi-avalanche" [12].

Up to now, only Er^{3+} with $\beta \cong 10^{-6}$ has shown, at room temperature, all the three characteristic features of avalanche as well when doping a $LiYF_4$ crystal or a ZBLAN fluoride glass both in bulk and in a fibre shape (see Sec. 4); even the long delay of several seconds to minute was observed [1–5]. For comparison the following values for the critical parameter have been given: for Nd^{3+}–$LiYF_4$, $\beta = 1.7 \times 10^{-4}$ for avalanche at $T < 40$ K [17, 21]; for Tm^{3+}–Ho^{3+}–$Gd_2Ga_5O_{12}$, $\beta = 3.6 \times 10^{-2}$ for the two-ion looping process [24]; for a Tm^{3+}BIGaZYTZr glass, $\beta = 1.2 \times 10^{-2}$ [25] for what was claimed to be "avalanche" at 100 K [13]. In the last case because the delay reaches only sixteen times [25] the metastable state lifetime (W_2^{-1}), we believe it to be a looping process case. In Er^{3+}, as it shall be possible to see from Secs. 4 and 5, the avalanche delay reaches 6×10^2 to 10^4 times W_2^{-1}, respectively, for fluoride glass and crystal.

4. Experiments in Er^{3+}-$LiYF_4$

In the case of Er^{3+}, the first step for photon avalanche has been clearly identified and attributed to anti-Stokes multiphonon side-bands absorption [1, 5] (see Fig. 6). Calculating the β ratio from mutiphonon absorption, allows one to estimate a value of 5×10^{-6} [4, 5], as shown in Fig. 7 which displays the multiphonon side-bands absorption in the avalanche excitation region. As observed, such experimental situation provides a clear threshold behaviour in the erbium case [1].

The simple theory of Sec. 3.1. has been verified by experimentally measuring $G(R_2)$. This was done using the following method (see Fig. 8): having obtained a given green output for a pump R_2 with $\Phi_{IR} = 0$, R_2 is reduced while increasing Φ_{IR} in order to maintain a constant green output. Φ_{IR} is an infrared signal at 0.94 μm in resonance with the metastable state 2 (here $^4I_{11/2}$) absorbing with a cross-section σ_0.

Each point is obtained after waiting for a steady state. Because of the large ratio for σ_0/σ_1 this experiment provides a good description of $G(R_2)$, as shown by results in Fig. 9 for three temperatures. We can define an R_{2C} asymptote only at 300 K and 220 K, respectively, 120 mW and 240 mW. At 163 K one cannot reach asymptote at our maximum available power of 250 mW. So the effect of lowering temperature is essentially to increase R_{2C}.

The part in R_{2C} which is most sensitive to temperature is C because it is related to phonon energy of only 100 cm^{-1}, whereas W_2 and W_3 are related to phonons covering the energy gap below level 3 and 2, that is energies > 2000 cm^{-1}. However this requires C to be of the same order as W_3 or bW_3, otherwise, as long

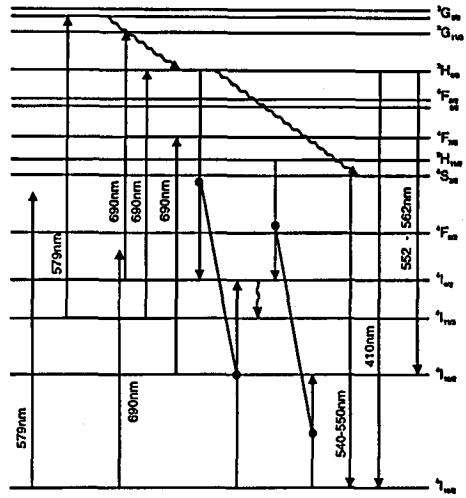

Fig. 6. Energy scheme of Er^{3+} and principal mechanisms responsible for photon avalanche cycles under excitation at 579 nm and 690 nm.

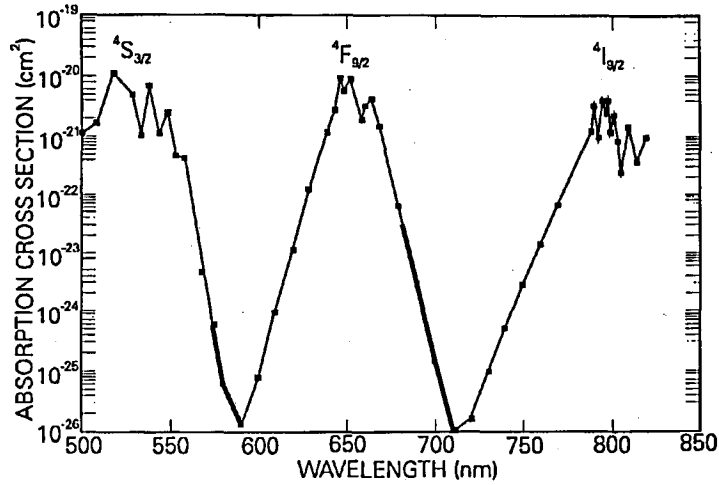

Fig. 7. Absorption cross-section for Er^{3+}–$LiYF_4$ taking into account the multiphonon contribution, the heavier lines show the anti-Stokes zones, which contribute to W_1 for the avalanche processes in erbium, [5].

as $C \gg W_3$, bW_3, one has $R_{2C} \cong W_2$ and its temperature dependence is just the same as W_2.

Comparing the theoretical threshold as given by Eq. (6′) with our experimental conditions we can verify our simple model.

We assume level 1 to be $^4I_{15/2}$, level 2 to be $^4I_{11/2}$ and level 3 to be the aggregation of levels between $^2G_{9/2}$ and $^4S_{3/2}$ with the emission properties of $^4S_{3/2}$

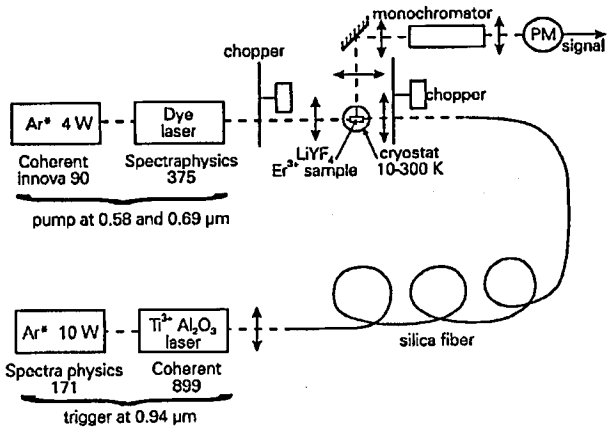

Fig. 8. Experimental scheme for measuring the positive feed-back gain.

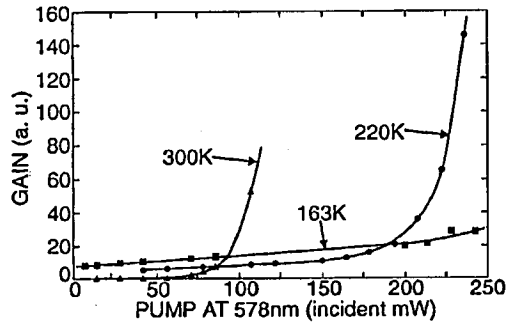

Fig. 9. Experimental $G(R_2)$ for three temperatures: 300 K, 220 K, 163 K, the residual signal near $R_2 = 0$ comes from the direct up-conversion under 0.94 μm excitation, [5].

(see Fig. 6). Taking the room temperature values given by Refs. [26, 27] we have the following parameters: $W_3 = 2500\ s^{-1}$, $b = 0.5$, $C = 0.5 \times 10^6\ s^{-1}$, $W_2 = 140\ s^{-1}$, because corresponding oscillator strengths are nearly equal ($\approx 0.4 \times 10^{-6}$) [27], we assume $\sigma_2 = \sigma_0 = 4 \times 10^{-21}\ cm^2$.

Using the reduced population units (pure number) we have $R_{2C} = 140(5 \times 10^5 + 2500)/(5 \times 10^5 - 1250) = 141\ s^{-1} \cong W_2$ (at room temperature) from which we have

$$\Phi_{\text{threshold}} = 141/(4 \times 10^{-21}) = 3.5 \times 10^{22} s^{-1}\ cm^{-2},$$

which at 0.578 μm gives for a 50 μm diameter spot a threshold power of $P_{\text{th}} = 222$ mW. This value is of the same order as the observed threshold values for 0.578 μm pumping.

$G(R_2)$ shows that we have a "marginally stable" positive feed-back system: even below the R_{2C} asymptote, we know from the feed-back system behaviour that a strong input signal can drive the system otherwise stable into its instability state (existence of a "gain stability margin").

In order to verify this behaviour we experimentally consider the case where, besides the input signal R_1/W_2 given by the pump, we added a pulsed trigger of amplitude $\sigma_0\Phi_{IR}/W_2$.

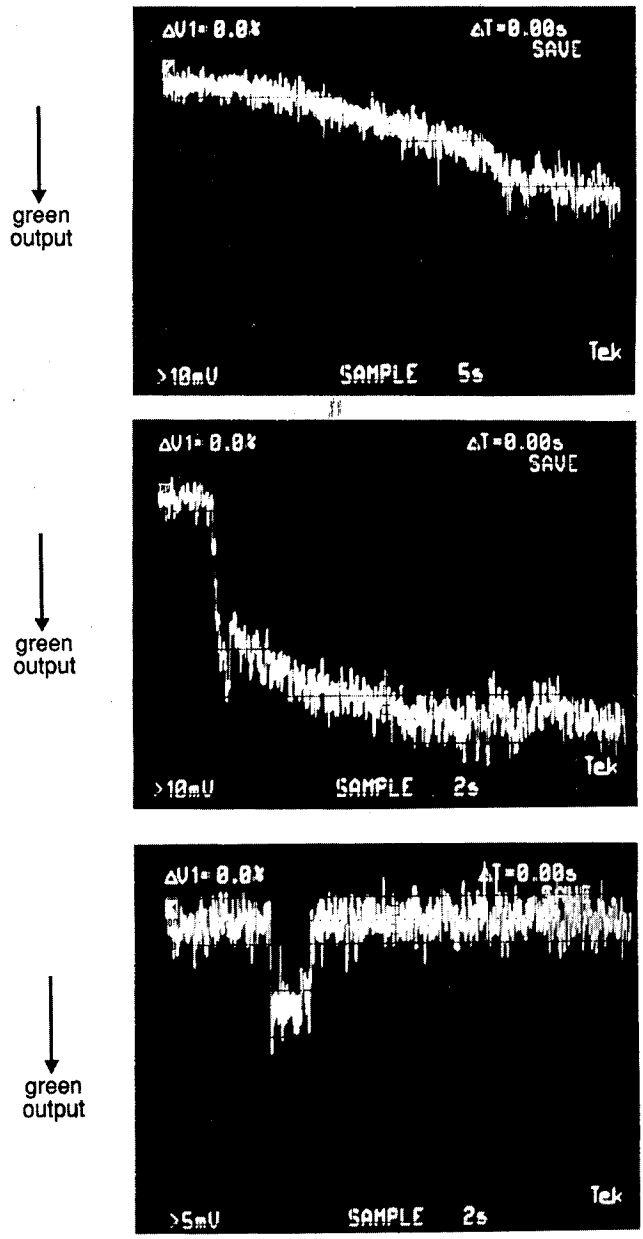

Fig. 10. Avalanche behaviour just below the threshold without (a) and with (b) a trigger feeding the metastable state and (c) much below the threshold, [5].

The results at room temperature are given in Fig. 10. In absence of trigger, with $P_p = 114$ mW at 578 nm incident on the sample, the threshold is reached after a very long time (> 50 s) (Fig. 10a). With the same pump intensity ($P_p = 114$ mW) and with a short trigger of 0.6 s, the avalanche state is obtained quickly and maintained after trigger extinction (Fig. 10b). With the same trigger but with a reduced pump ($P_p = 99$ mW) the avalanche state is not reached. The behaviour of Fig. 10a,b,c is obtained down to 180 K.

At temperature lower than 180 K the observed threshold certainly increases (Fig. 9). However, as our temperature scan has a relatively short time constant (3 s/K from 10 to 50 K, then 21 s/K from 50 to 150 K) we are not sure that the threshold could not be reached for an avalanche delay time ≥ 50 s.

From this experiment we understand that measuring a threshold depends on the time we are ready to wait for before its observation and this time depends not only on excited state pumping but also on the ground state absorption conditions. In any case, below 180 K being then limited by the pump laser at a much lower power than the threshold, we obtain the result shown in Fig. 10c. Such triggering effect realises an optical analogue of a thyratron.

The time delay behaviour of the avalanche process has been studied theoretically quite recently within the general model of Landau for phase transition [25]. The time delay at the threshold, in fact a "critical slowing time", t_c, proved itself to be the most sensitive experimental data when looping or avalanche takes place. It has been shown to be given by [25]

$$t_c = K\sqrt{\sigma_2/\sigma_1}, \tag{7}$$

where K depends on other spectroscopic parameters. Equation (7) is rather well verified in our experiments for which avalanche delay times have been determined for two different excitation wavelengths of well-known multiphonon anti-Stokes cross-sections: at $\lambda = 688$ nm, $\sigma_1 = 10^{-24}$ cm^2, a delay is found to be 0.4 s; whereas at $\lambda = 579$ nm, $\sigma_1 = 2 \times 10^{-26}$, and a delay is 4 s. Assuming for σ_2 the same value in both cases of excitation, the ratio of delays is 0.1 which is in rather good accord with the value of 0.14 as given by Eq. (7).

Above the threshold, the delay for avalanche has been given by Ref. [7] as:

$$t_c = kW_2^{-1}/(\Phi/\Phi_C - 1) \tag{8}$$

with $k = W_3^{-1}/(1+b)(2c+W_3)$, and where $\Phi_C = R_C/\sigma_2$ is the pumping flux at the threshold and Φ — the effective pumping flux.

5. Photon avalanche in Er^{3+}-fluoride glasses in fibre and bulk shape

Recently, the photon avalanche effect has been observed in a Pr^{3+}-doped silica fibre [11] and in an Er^{3+}-doped fluoride glass fibre [2,4], in both cases at room temperature. In the first case, only the transmission non-linearity is observed and not the up-conversion emission threshold. It was believed that the threshold was so low that it could not be observed. We think that this is explained by the too strong non-resonant to resonant absorption ratio as mentioned in Sec. 3.2. On the opposite in the second case, the clear thresholds at 5 mW and at 4 mW of incident power at respectively 579 nm [4] and 690 nm [2] are observed because in these last two cases, the first step is a weak anti-Stokes multiphonon absorption

giving again a β ratio of about 10^{-6} much below the critical value of 10^{-4}. The involved energy scheme for both excitations is essentially the same as in Fig. 6; it shows both pumpings and the two types of involved cross-relaxations. Figure 11 presents the typical threshold behaviour for the up-conversion emission. The long delay behaviour is displayed in Fig. 12 showing, near the threshold, the very long time of 3.5 s, which is largely in excess of any of the lifetimes of the metastable states of erbium. The observed delay follows rather well the behaviour predicted by Eq. (8).

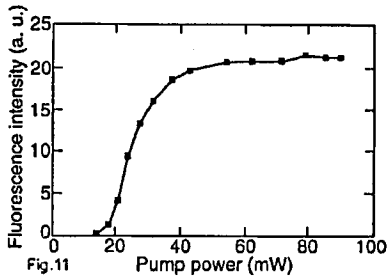

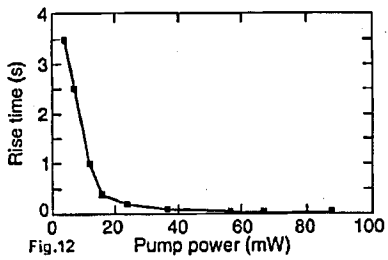

Fig. 11. Up-conversion emission at 550 nm showing the existence of the avalanche threshold in a ZBLAN: Er^{3+} fibre observed from its extremity, [4].
Fig. 12. Time delay for the avalanche establishment versus incident pump power at 579 nm in a ZBLAN: Er^{3+} fibre, [4].

The same results can be obtained for glass and bulk samples [1, 2]. Because the first absorption step, being of a multiphonon nature, is featureless, the excitation spectrum for avalanche provides directly with a single excitation beam the ESA spectrum of the resonant second absorption as shown in Fig. 13 for the $^4I_{11/2}$–$^2G_{9/2}$ transition of Er^{3+}. This gives a new method [3] to reach ESA spectra otherwise difficult to obtain.

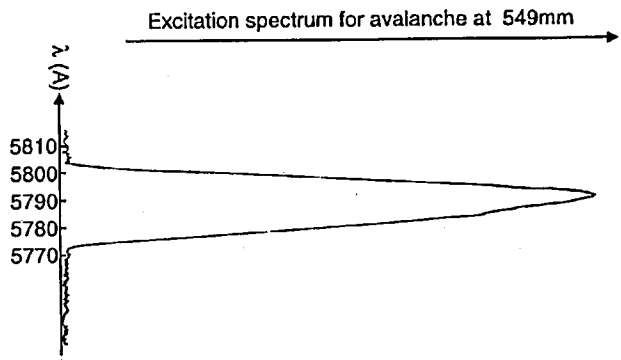

Fig. 13. Excitation spectrum for the avalanche emission at 549 nm in a ZBLAN:Er^{3+} glass showing the spectrum for the $^4I_{11/2}$–$^2G_{9/2}$ ESA transition, [3].

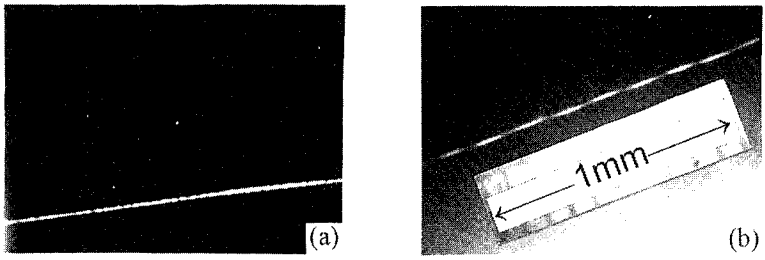

Fig. 14. Spatial domains observed along the fibre above the photon avalanche threshold: (a) dot separation about 1 mm; (b) microscope view of a 1 mm avalanche dot, the scale is 100 μm per division, [2].

The main difference with bulk samples is that in the fluoride fibre case, yet not completely explained, the up-conversion spatial domains appear with periodic structures with periods ranging from few cm to mm and 100 μm [2,4], as shown in Fig. 14.

6. Conclusion

The effective conditions for a clear observation of the rather puzzling photon avalanche effect have been recalled. It has been shown that an erbium ion in fluoride matrices fulfills these conditions so well that this effect is particularly spectacular in such systems even at room temperature. It is striking that a system in the solid state ($LiYF_4$) can display a delay of quantum origin as long as 50 s, corresponding to about 10^4 cycles (t_c/W_2^{-1}) in the feed-back loop. Though avalanche pumping of lasers have been demonstrated [6,7,16], and even ASE in Er^{3+}-doped fibre [28], Fig. 5 shows that the population n_3 is always higher in ESA than in avalanche for the given pumping rate R_2. This shows that avalanche is not such an effective way of pumping laser except when a double resonance is not readily available for one pumping wavelength.

Acknowledgment

I would like to thank my former collaborators, Yi Hong Chen and Daniel Meichenin, who have participated actively in the works presented here, and my present collaborators, Fabienne Pellé and Philippe Golner, for making some of their results available prior to publication.

References

[1] F. Auzel, Y.H. Chen, D. Meichenin, ICL'93, Storrs, CN, USA, 9–12 August 1993; *J. Lumin.* **60/61**, 692 (1994).

[2] Y.H. Chen, F. Auzel, *Electron. Lett.* **30**, 323 (1994).

[3] F. Auzel, Y.H. Chen, *J. Non-Crystal. Solids* **184**, 57 (1995).

[4] Y.H. Chen, F. Auzel, *J. Phys. D, Appl. Phys.* **28**, 207 (1995).

[5] F. Auzel, Y.H. Chen, *J. Lumin.* **65**, 45 (1995).

[6] J.S. Chivian, W.E. Case, D.D. Eden, *Appl. Phys. Lett.* **35**, 124 (1979).

[7] W.E. Case, M.E. Koch, A.W. Kueny, *J. Lumin.* **45**, 351 (1990).

[8] M.E. Koch, A.W. Kueny, W.E. Case, *Appl. Phys. Lett.* **56**, 1083 (1990).

[9] R. Scheps, *IEEE* **QE30**, 2914 (1994).

[10] R. Scheps, *IEEE* **QE31**, 309 (1995).

[11] A.S.L. Gomes, G.S. Maciel, R.E. de Araujo, L.H. Acioli, C.B. de Araujo, *Opt. Commun.* **103**, 361 (1993).

[12] P. Goldner, F. Pellé, *Optical Materials*, to be published, (1995); F. Pellé, P. Goldner, *Acte Phys. Pol. A* **90**, 197 (1996).

[13] M.F. Joubert, S. Guy, C. Linares, B. Jacquier, J.L. Adam, *J. Non-Cryst. Solids* **184**, 98 (1995).

[14] A. Brenier, L.C. Courrol, C. Pédrini, C. Madej, G. Boulon, *J. Lumin.* **58**, 285 (1994).

[15] J.M. Dyson, S.M. Jaffe, H. Eilers, M.L. Jones, W.M. Dennis, W.M. Yen, *J. Lumin.* **60/61**, 668 (1994).

[16] N.J. Krasutsky, *J. Appl. Phys.* **54**, 1261 (1983).

[17] W. Lenth, R.M. Macfarlane, *J. Lumin.* **45**, 346 (1990).

[18] U. Oetliker, M.J. Riley, P.S. May, H.U. Güdel, *J. Lumin.* **53**, 553 (1992).

[19] H. Ni, S.C. Rand, *Opt. Lett.* **17**, 1222 (1992).

[20] N. Pelletier-Allard, R. Pelletier, *Phys. Rev. B* **26**, 4425 (1987).

[21] M.F. Joubert, S. Guy, B. Jacquier, *Phys. Rev. B* **48**, 10031 (1993).

[22] A.W. Kueny, W.E. Case, M.E. Koch, *J. Opt. Soc. Am. B* **10**, 1834 (1993).

[23] A. Brenier, G. Boulon, C. Madej, C. Pédrini, L. Lou, *J. Lumin.* **54**, 271 (1993).

[24] A. Brenier, L.C. Courrol, C. Pédrini, C. Madej, G. Boulon, *Opt. Mater.* **3**, 25 (1994).

[25] S. Guy, Ph.D. Thesis, Université Claude-Bernard-Lyon I, 1995.

[26] J. Rubin, A. Brenier, R. Moncorgé, C. Pédrini, *J. Lumin.* **36**, 39 (1986).

[27] S. Hubert, D. Meichenin, B. Zhou, F. Auzel, *J. Lumin.* **50**, 7 (1991).

[28] Y.H. Chen, F. Auzel, *Electron. Lett.* **30**, 1602 (1994).